PHYSICAL REVIEW B **78**, 075416 (2008)

Optical anisotropies of metal clusters supported on a birefringent substrate

J. M. Flores-Camacho, L. D. Sun, N. Saucedo-Zeni, G. Weidlinger, M. Hohage, and P. Zeppenfeld*
Institut für Experimentalphysik, Johannes Kepler Universität Linz, Altenbergerstrasse 69, A-4040 Linz, Austria
(Received 28 November 2007; revised manuscript received 30 May 2008; published 13 August 2008)

We report on the optical properties of Ag nanoparticles supported on an insulating, birefringent substrate for nominal film thicknesses of less than 4 nm. Spectroscopic ellipsometry (SE) and reflectance-difference spectroscopy (RDS) were employed to detect out-of-plane and in-plane anisotropies of particle-plasmon resonances, respectively. Quantitative agreement between measured and calculated spectra is achieved using the morphological parameters determined independently from electron microscopy images. The substrate birefringence allows the detection of cluster layers by RDS via the screening of the substrate signal proportional to the layer susceptibility. In addition, an intrinsic lateral anisotropy, which is explained by the lifting of the degeneracy of planar modes due to the anisotropic images forming in the substrate, has been detected. For higher coverages the influence of anisotropic cluster shapes and strong multipolar resonances are identified.

DOI: 10.1103/PhysRevB.78.075416 PACS number(s): 78.67.Bf, 78.68.+m, 78.20.Fm, 73.20.Mf

I. INTRODUCTION

Nanometer sized metal particles have recently attracted much scientific interest due to their promising applications in catalysis, ultrahigh data storage, and biomolecular sensors. Access to their physical properties can be gained via optical means by probing the particle-plasmon polariton resonances, i.e., the excitation by light of collective electron motion.[1,2] In the case of nanoparticles supported on a substrate, the optical response is manifested in form of resonances with different spectral positions corresponding to plasmon modes polarized perpendicular (1,0) and parallel (1,1) to the substrate.[3–5] In the following we will refer to this kind of splitting as *out-of-plane* anisotropy. Under certain conditions the otherwise degenerate planar modes (1,1) can also be split;[6–9] this second class of anisotropy will be referred to as *in-plane* anisotropy.

In this paper, we present a characterization by means of *ex situ* spectroscopic ellipsometry (SE) and *in situ* reflectance-difference (-anisotropy) spectroscopy (RDS/RAS) of nominally few nanometer thick layers of Ag clusters supported on a laterally anisotropic $Al_2O_3(10\bar{1}0)$ substrate. This combination of SE and RDS allows us to selectively study out-of-plane and in-plane anisotropies, respectively.

SE probes the change in polarization state upon oblique reflection of linearly polarized incident light [Fig. 1(a)]. The splitting between the (1,0) and (1,1) modes can have different origins, such as the oblateness of the particle,[10] truncation of the figure,[11,12] and even the filling fraction in a two-dimensional distribution of particles.[5,13] Besides SE,[14] several other techniques such as extinction/absorption,[2,4] reflectivity,[15] and surface differential reflectance (SDR) (Ref. 16) are sensitive to the out-of-plane anisotropy.

RDS (Refs. 17–20) measures the difference in reflectivity at normal incidence for two orthogonal, linear polarizations of the incident light, E_x and E_y, which are aligned with the in-plane optical eigenaxes of the sample [see Fig. 1(b)]. The acquired signal can be written as

$$\frac{\Delta r}{r} = 2\frac{r_x - r_y}{r_x + r_y}, \tag{1}$$

where r_δ is the complex reflection coefficient for light polarized along the in-plane δ eigenaxis of the sample. In the following, $\delta\ (=x,y,z)$ will be used as the laboratory frame.

Due to the normal incidence of light $\Delta r/r$ is a measure of the lateral anisotropy of the system, which in the present case consists of small metal particles on top of an anisotropic substrate. Therefore, the optical anisotropy arises from both the intrinsic optical anisotropy of the cluster layer, giving rise to a splitting of the in-plane (1,1) plasmon resonance, and from the overlayer induced modulation of the anisotropic substrate response, similar to the screening due to roughness in surfaces of bare materials[21,22] or adsorbed species on anisotropic substrates.[23] As we will show in this paper, this *screening contribution* produces most of the anisotropy signal for overlayers with strong plasmon-related features. Nevertheless, the different contributions to the reflectance-difference (RD) signal can be properly analyzed and the part of the spectrum that corresponds to the *intrinsic* causes of anisotropy of the cluster layer can thus be separated from the screening contribution. Note that the (1,0)

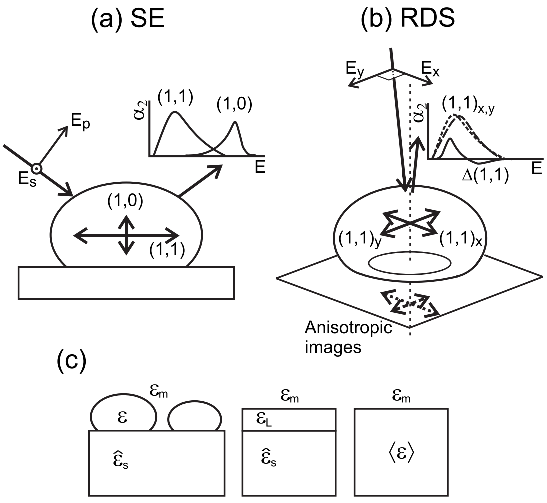

FIG. 1. Metal cluster optical anisotropies measured by (a) SE and (b) RDS. The complementary information obtained in the two cases is shown schematically in terms of the imaginary part of the polarizabilities $\mathrm{Im}(\alpha)=\alpha_2$. (c) Sample representations with the definitions used in the paper.

1098-0121/2008/78(7)/075416(9)

plasmon resonance is polarized perpendicular to the substrate and cannot be excited at normal incidence of light. Consequently, RDS can be used as a measure of the small in-plane anisotropies without the influence of the out-of-plane (1,0) mode.

The intrinsic lateral anisotropy in the optical response of metal clusters supported on a substrate can have different sources: it can be caused directly by the shape of the particle (anisotropic shape, SH), e.g., if the particle resembles an ellipsoid where the lengths of the in-plane axes are different.[7,8,24] Alternatively, the anisotropy can be caused indirectly by anisotropic interactions between the particles (anisotropic interaction, IN) if they are arranged in a pattern of lower than square symmetry[6,25] or by the strong interaction in particle pairs.[26] As we will demonstrate in this paper, another indirect cause for the optical anisotropy is the development of an effective anisotropic polarizability of the particle in response to a substrate with a laterally anisotropic dielectric function (anisotropic images, IM). Müller *et al.*[27] and Park and Stroud[28] reported a similar situation in which a spherical particle embedded in a polarized nematic matrix has been described as behaving optically as a spheroid without actually being distorted.

II. EXPERIMENT

The Ag clusters were prepared in a UHV chamber (base pressure $p \leq 5 \times 10^{-10}$ mbar) by depositing Ag onto $\mathrm{Al_2O_3}(10\bar{1}0)$ substrates (from SurfaceNet) at room temperature by means of an EFM3i UHV-evaporation source supplied by Omicron/Focus. A controlled Ag deposition rate of 0.1 nm/min was used. The dielectric response ε_s and the anisotropy $\Delta\varepsilon_s = 0.03$ of the back-side roughened $\mathrm{Al_2O_3}(10\bar{1}0)$ substrates were measured before Ag deposition by SE and RDS.

For the *in situ* characterization of the cluster layers we used an RD spectrometer from Horiba Jobin Yvon in the Acher-Drévillon configuration.[18] The spectrometer was attached to the UHV chamber through a low-strain window. The photon energy range is 1.5–5.5 eV.

Ex situ characterization was carried out by means of RDS and a variable angle of incidence M-2000 rotating compensator spectroscopic ellipsometer from J. A. Woollam Co. The multichannel ellipsometer has a photon energy range of 1.2–5 eV.

The morphology of the cluster layer was determined by means of a LEO supra 35 scanning electron microscope (SEM) from Raith.

III. MODEL

A. Spectroscopic ellipsometry

Given the small size of the particles involved in the present work, we will restrict ourselves to the quasistatic approximation. The polarizability of an ellipsoidal particle embedded in a medium with dielectric function ε_m ($\varepsilon_m = 1$ for vacuum or air) is given by[2,29]

$$\alpha_\vartheta = \frac{R_X R_Y R_z}{3} \frac{\varepsilon - \varepsilon_m}{\varepsilon_m + L_\vartheta(\varepsilon - \varepsilon_m)}, \tag{2}$$

where $\vartheta = (X, Y, z)$ and R_X, R_Y, and R_z are the radii of the particle along its major axes (the frames ϑ and δ are related by a rotation around z). ε is the bulk dielectric function of the particle material (silver) whose imaginary part has to be corrected to account for the reduced electron relaxation time due to the limited size of the particle,[30] and L_ϑ are the shape depolarization factors.[2] For an oblate spheroid $R_X = R_Y = R_\parallel$, $L_X = L_Y$, and $\alpha_X = \alpha_Y = \alpha_\parallel$.

The polarizabilities have to be transformed into the anisotropic surface susceptibility tensor[3] with principal components (γ, γ, β) by formally taking into account the truncation of the spheroid, the interaction between particles, and the interaction with the substrate[31] up to quadrupolar order. However, in the dipolar approximation[4,5] the picture can be simplified and the truncation enters in the self-image term of Ref. 5 as $S_z^2/(4ft^3)$, where $S_z = R_\parallel / R_z$ is the aspect ratio, $t = D/R_z$ is the truncation of the spheroid, with $2D$ as the distance between the direct dipole and its image, and $f = \rho\pi R_\parallel^2$ is the two-dimensional filling fraction, with ρ as the number of particles per unit area.

For dilute systems $\gamma = \rho\bar{\alpha}_\parallel$ and $\beta = \rho\bar{\alpha}_z$ ($\varepsilon_m = 1$), i.e., a simple average of the responses of noninteracting particles, but for medium coverages the surface susceptibility has to account for at least dipolar interactions. These are usually included in models assuming particles arranged in a square lattice or for random distributions within the framework of the mean field approximation (MFA). The randomness of the system induces further broadening and splitting of the modes, which are underestimated by the MFA. In our case we adapted the renormalized polarizability theory[5] (RPT) to account for the oblateness of the particle. RPT considers the variance of the dipole-dipole interaction tensor caused by randomness in the positions of the clusters which leads to the coupling of the cluster eigenmodes.[29]

As will be discussed in the following sections, SE spectra were measured in ambient air, thus the effects of tarnishing ought to be considered. To this end we used the polarizability of a particle coated by a dielectric shell (Sec. 5.4 of Ref. 2) instead of Eq. (2). If the shell and the core have the same aspect ratio the net polarizability can be written as

$$\alpha_\vartheta = \frac{V_p}{4\pi} \frac{(\varepsilon_p - 1)[\varepsilon_p + (\varepsilon - \varepsilon_p)(1 - f_v)L_\vartheta] + f_v\varepsilon_p(\varepsilon - \varepsilon_p)}{[\varepsilon_p + (\varepsilon - \varepsilon_p)(1 - f_v)L_\vartheta][1 + (\varepsilon_p - 1)L_\vartheta] + f_v L_\vartheta \varepsilon_p(\varepsilon - \varepsilon_p)}, \tag{3}$$

where ε_p is the dielectric function of the shell, V_p is the volume of the coated cluster, and $f_v = R_\parallel^3/(R_\parallel + d_p)^3$ is the volumetric fraction of the particle occupied by the core. The shell thickness d_p can be positive or negative indicating added material (contamination) or tarnishing (e.g., oxidation) of the outer rim, respectively. As with Eq. (2), the truncation parameter is introduced externally as a perturbation to the dipole formed in the cluster. The fact that Eq. (3) was originally developed for completely surrounded particles and that it assumes well-defined interfaces constitutes a limitation for the present application. However, for the given conditions of the shell (transparency and small thickness) it is still a viable approximation.

Finally, the effective dielectric function $\langle\varepsilon\rangle=\langle\varepsilon_1\rangle+i\langle\varepsilon_2\rangle$ of the layer/substrate system as a whole, as measured in SE, is obtained by introducing in the ellipsometry formulas[32] the reflection coefficients according to the thin-film theory,[3,10,33,34]

$$r_s=\frac{\cos\theta-n_s\cos\theta'+ik\gamma}{\cos\theta+n_s\cos\theta'-ik\gamma}, \tag{4}$$

$$r_p=\frac{(n_s\cos\theta-\cos\theta')\left(1-\dfrac{k^2}{4}\gamma\beta\sin^2\theta\right)-ik\gamma\cos\theta\cos\theta'+ikn_s\beta\sin^2\theta}{(n_s\cos\theta+\cos\theta')\left(1-\dfrac{k^2}{4}\gamma\beta\sin^2\theta\right)-ik\gamma\cos\theta\cos\theta'-ikn_s\beta\sin^2\theta}, \tag{5}$$

where θ and θ' are the angles of incidence and refraction, respectively, $n_s=\sqrt{\varepsilon_s}$ is the refractive index of the substrate, and $k=2\pi/\lambda$. In the rest of the paper we will choose the real or the imaginary part of the effective dielectric function $\langle\varepsilon\rangle$ to illustrate the apparent optical response of the whole sample, whereas the dielectric response of a particular layer or component of the system will be addressed when necessary [see Fig. 1(c)].

In Fig. 2 we show the output of the model in form of surface susceptibilities $\gamma=\rho\alpha_\parallel^*$ and $\beta=\rho\alpha_z^*$, where α^* is the renormalized polarizability, together with the real part $\langle\varepsilon_1\rangle$ of the effective dielectric function $\langle\varepsilon\rangle$ derived from r_s and r_p of Eqs. (4) and (5).[32] Note that $\langle\varepsilon_1\rangle$ peaks at the resonant energies of the loss functions Im(γ) and Im(β), corresponding to the excitation energies of the (1,1) and (1,0) plasmon modes, respectively. Thus the real part of the effective dielectric function of the whole system $\langle\varepsilon\rangle$ is directly related to the imaginary part of the cluster layer dielectric function ε_L. Indeed, in the long wave approximation the dimensions of the cluster and the separation distances are both much smaller than λ, and the cluster layer might be regarded as a continuous *flat* film with dielectric function ε_L. Thus in Eq. (5), $\beta\sim 1-\varepsilon_{L,z}^{-1}$.[10] On the other hand, the resulting effective dielectric function of the entire system $\langle\varepsilon\rangle$ is similar to $-i\varepsilon_L$ (with the factor $-i$ implying an interchange of the real and imaginary parts, as seen in Fig. 2). This is a consequence of having a stacked system where the material with the strongest spectral features lies on top of a transparent substrate with no pronounced spectral structure. The opposite sign of the (1,0) related plasmon peak in $\langle\varepsilon_1\rangle$ as compared to the (1,1) mode is a consequence of the discontinuity of the normal component of the field at the *interface* between the cluster layer and the external medium (vacuum).[35–37]

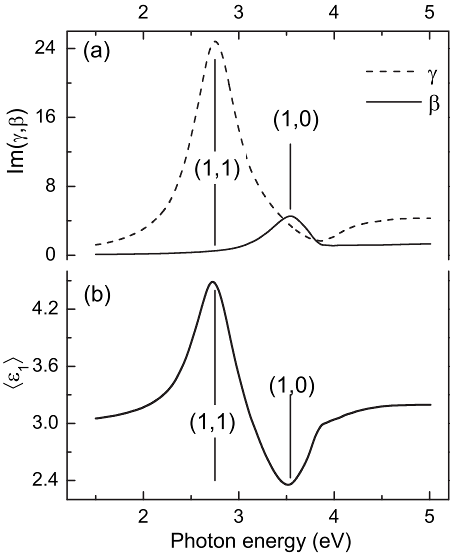

FIG. 2. Output of the SE model. (a) Surface susceptibilities calculated for Ag cluster layer with a nominal thickness of 1 nm on $Al_2O_3(10\bar{1}0)$ (parameters as in Table I) and (b) real part of the effective dielectric function of the whole system.

B. Reflectance-difference spectroscopy

RPT was adapted to include anisotropic substrates. In this case the originally isotropic contribution of the images $A=(\varepsilon_s-1)/(\varepsilon_s+1)$ has to be transformed as[38–40]

$$A\rightarrow\begin{pmatrix} A_a+\frac{3\Delta A}{2} & 0 & 0\\ 0 & A_a+\frac{\Delta A}{2} & 0\\ 0 & 0 & 2(A_a+\Delta A)\end{pmatrix}, \tag{6}$$

where

$$A_a=\frac{\varepsilon_a-1}{\varepsilon_a+1}, \tag{7}$$

$$\Delta A=\frac{\Delta\varepsilon}{2(\varepsilon_a+1)^2}, \tag{8}$$

corresponding to a uniaxial crystal with the c axis lying in the plane of the substrate surface. In our convention the components of the substrate dielectric tensor $\hat{\varepsilon}_s$ are $(\varepsilon_s)_{xx}=\varepsilon_c$, $(\varepsilon_s)_{yy}=(\varepsilon_s)_{zz}=\varepsilon_a$, and $\Delta\varepsilon_s=\varepsilon_c-\varepsilon_a$, implying that the RDS instrument was aligned to obtain maximum positive signal of the bare substrate (δ frame). As a consequence, the surface

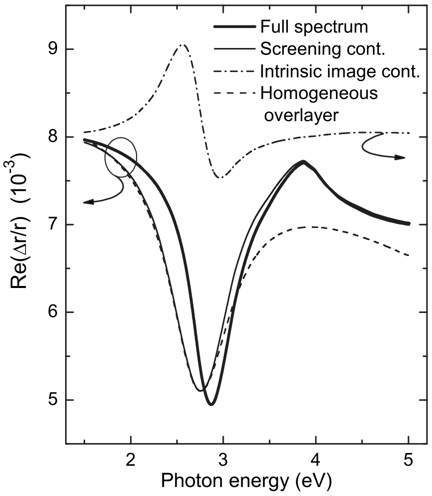

FIG. 3. Output of the RDS model. The thick line is the result of Eq. (10) for a 1 nm Ag cluster layer on $Al_2O_3(10\bar{1}0)$, whereas the thin and the dash-dotted lines are the screening and the intrinsic anisotropic image contributions according to Eq. (11) and Eq. $(12)|_{\mathrm{IM}}$, respectively. The dashed line shows the result for an effective homogeneous overlayer on top of anisotropic $Al_2O_3(10\bar{1}0)$ substrate obtained using the Abelès approach.

susceptibility becomes effectively in-plane anisotropic $(\gamma_x, \gamma_y, \beta)$ due to the local field induced by images forming in the birefringent substrate. The diagonal form of the tensor is retained.

The reflection coefficient r for light polarized along the in-plane direction δ impinging at normal incidence on a thin film of clusters on a substrate is

$$r_\delta = \frac{1 - n_{s,\delta} + ik\gamma_\delta}{1 + n_{s,\delta} - ik\gamma_\delta}, \tag{9}$$

where $n_{s,\delta}$ is the refractive index of the substrate along $\delta = x, y$ and $\gamma_\delta = \rho\alpha^*_\delta$ is the in-plane surface susceptibility considering the in-plane anisotropic renormalized polarizabilities α^*_δ. The RD signal is then obtained by substitution of Eq. (9) for polarizations of the incident light along the x and y eigenaxes of the substrate in Eq. (1),

$$\frac{\Delta r}{r} = -2\frac{\Delta n_s - ik\Delta\gamma}{1 - (n_{s,x} - ik\gamma_x)(n_{s,y} - ik\gamma_y)}. \tag{10}$$

Equation (10) contains two sets of contributions, namely,

$$\left.\frac{\Delta r}{r}\right|_{\Delta\gamma=0} = \frac{-2\Delta n_s}{1 - (n_{s,x} - ik\gamma)(n_{s,y} - ik\gamma)}, \tag{11}$$

$$\left.\frac{\Delta r}{r}\right|_{\Delta n_s=0} = \frac{2ik\Delta\gamma}{1 - (n_s - ik\gamma_x)(n_s - ik\gamma_y)}. \tag{12}$$

Equation (11) describes the effect of the presence of a cluster layer with in-plane isotropic plasmon resonances on top of an anisotropic substrate, which we will refer to as the *screening effect* (see Fig. 3). This contribution can also be well reproduced using the Abelès approach for a homogeneous overlayer as will be described below.

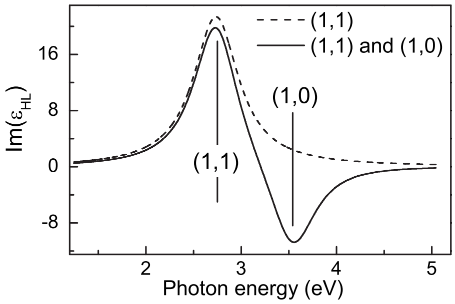

FIG. 4. Imaginary part of the apparent dielectric function of a homogeneous overlayer (HL) which has been extracted from the experimental data in Fig. 6 using a three-phase model.

The different intrinsic anisotropies can be described by means of Eq. (12). Although Eq. (12) was developed in the present work for anisotropic images via Eq. (6) and thus we should have formally written $\Delta\gamma^{\mathrm{IM}}$, we would like to emphasize its generality as it can also be used for the other intrinsic sources of anisotropy described in Sec. I. In fact, Eq. (12) is of the same form as Eq. (3) in Ref. 8 derived for elliptical cluster shapes $(\Delta\gamma^{\mathrm{SH}})$. In Fig. 3 we present the output of the calculations for the same set of parameters used in Fig. 2 illustrating the different contributions to the full spectrum for the case of anisotropic images $[\mathrm{Eq.}\ (10) \equiv \mathrm{Eq.}\ (11) + \mathrm{Eq.}\ (12)|_{\mathrm{IM}}]$. From the comparison of the curves in Fig. 3 with the (1,1) mode in Fig. 2(a) we observe that Eq. (11) $\propto -\mathrm{Im}(\alpha_\parallel)$ as discussed above in the context of Fig. 2 and that Eq. (12) is dominated by a contribution $\propto -d\,\mathrm{Im}(\alpha_\parallel)/dE$ (with ρ included in the proportionality factor). The latter relationship is a consequence of the anisotropy term $\Delta\gamma$ in Eq. (12) and reminiscent of the so-called *derivative model* often evoked in the context of the three-phase model in RDS.[41]

C. Three layer model and Abelès approach

Simplified phenomenological models can be used for comparison with the results of those simulations based on a realistic description of the cluster layer described above. In particular, we can obtain, in an alternative way, the screening contribution to the RD spectrum using a three-phase model (vacuum/HL/anisotropic substrate) where HL stands for a hypothetical isotropic homogeneous layer with a constant width corresponding to the nominal thickness of the cluster layer (1 nm in Fig. 3) but with an effective dielectric function which includes all relevant plasmonic excitations.

In a first step, the effective dielectric function of the overlayer $\varepsilon_{\mathrm{HL}}$ was extracted directly from the experimental SE data (Fig. 6) using the built-in routines of the spectrometer to convert the ellipsometric data on the basis of a three-phase model (vacuum/1 nm HL/isotropic substrate). Thus, in this first step, the anisotropy of the substrate is neglected but will be reintroduced below in the actual calculation of the screening effect. For the isotropic substrate dielectric function we used the average value of the measured anisotropic response of $Al_2O_3(10\bar{1}0)$, which is a good approximation given that $\Delta\langle\varepsilon\rangle \ll \langle\varepsilon\rangle$. The result is plotted in Fig. 4 along with a fit by two Lorentzians corresponding to the (1,1) and (1,0) modes.

As already discussed in the context of Fig. 2, the extracted effective dielectric function $\varepsilon_{\mathrm{HL}}$ may exhibit negative peaks and even unphysical negative values in its imaginary part, here associated with the (1,0) resonance.

Next, we have used the Abelès approach[32] to estimate the screening contribution to the RD signal, explicitly taking into account the measured dielectric anisotropy of the substrate. To this end the system is modeled by an isotropic homogeneous layer ($j=1$) with an effective optical response described by the (1,1) curve of Fig. 4 on top of the anisotropic $\mathrm{Al_2O_3}(10\bar{1}0)$ substrate ($j=2$), surrounded by vacuum or air ($j=0$). Note that we only retained the Lorentzian contribution corresponding to the (1,1) mode in $\varepsilon_{\mathrm{HL}}$ (dashed line in Fig. 4) since only this resonance can be excited in the RDS geometry for normal incidence of light. In the Abelès approach the light propagating through each layer j of a stacked optical medium is represented by the product of the Jones matrix describing the layer L_j and the reflection/transmission coefficients at the interfaces $I_{j,j+1}$.[32] The advantage of this method is that the anisotropy of any of the layers can be easily introduced in its Jones matrix. The Fresnel coefficients for the δ polarization of the light are obtained as $r_\delta = S_{\delta,(2,1)}/S_{\delta,(1,1)}$, where the scattering matrix $S=I_{0,1}L_1I_{1,2}$ (omitting the subscript δ for the two polarization directions) and the subscripts in the parentheses denote matrix elements.

Finally, the RD signal is calculated by substituting these Fresnel coefficients for normal incidence in Eq. (1). The result is shown in Fig. 3 along with the outputs of the RDS simulations described in Sec. III B. The screening contribution to the RD signal is well reproduced using the homogeneous overlayer model, as can be seen by the overlapping of the corresponding curves at the vicinity of the peak in Fig. 3. The deviations at higher energies result from the fact that the effective homogeneous overlayer dielectric function was derived from the experimental SE data by assuming a simple Lorentzian line shape for the isotropic (1,1) mode (Fig. 4).

IV. RESULTS

The morphology of the cluster layers, as determined by SEM and the analysis performed with the aid of image-analysis programs,[42,43] is presented in Figs. 5(a)–5(c). Figure 5(d) displays the Feret radius (R_F), defined as is the radius of a circle with the same area as the actual cluster, versus the major semiaxis of the cluster R_M. The dashed line depicts the trend for the present range of cluster sizes. The deviation from the line of perfect circles (solid line) which increases with cluster size is a clear evidence for an elongation, of the larger particles, though not necessarily for their preferential orientation or alignment. Whether this elongation occurs randomly or preferentially along a certain direction can be inferred from the fast Fourier transform (FFT) images presented in the right panels of Figs. 5(a)–5(c): from the ringlike structure in the FFT image of Fig. 5(a) we conclude that the cluster shape and arrangement for the 1 nm Ag sample is laterally isotropic. Thicker cluster layers (3 and 3.8 nm Ag), however, are characterized by a weak but non-negligible ellipsoidal shape in the FFT images [Figs. 5(b) and 5(c)] indicating that either the cluster elongation or their alignment occurs preferentially along the direction indicated by the dashed lines in the FFT images. Evident alignments of Ag clusters on $\mathrm{Al_2O_3}(10\bar{1}0)$ have been reported previously.[25,44]

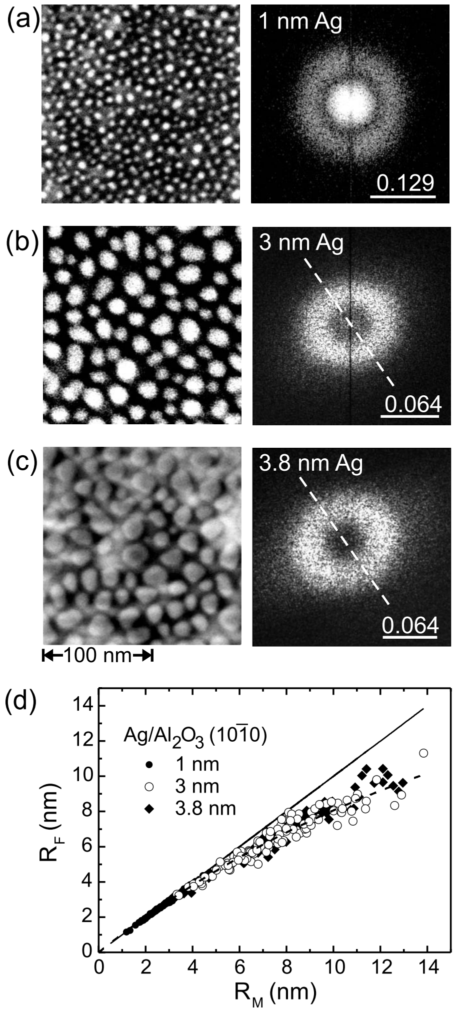

FIG. 5. [(a)–(c)] Real space SEM images and calculated reciprocal space power spectra (FFT) for 1, 3, and 3.8 nm $\mathrm{Ag/Al_2O_3}(10\bar{1}0)$, respectively. Scales are indicated (FFT in nm^{-1}). (d) Feret radius R_F plotted against the cluster major semiaxis length R_M. The solid line (slope=1) represents clusters growing with an in-plane circular shape.

Since the out-of-plane anisotropy is better known in the literature, we first present our SE results expressed in terms of an effective dielectric function $\langle \varepsilon \rangle$ for the different samples (Fig. 6). Two situations are considered, according to whether the samples were measured before or after SEM characterization, which imply different degree of tarnishing or contamination. The differences are clearly evident in the direct comparison of both stages for the 1 nm Ag layer. Also shown are simulations of the experimental SE spectra based on the model described in Sec. III A. The geometrical cluster parameters were extracted from the SEM images in Fig. 5. For the dielectric function of silver we used experimental

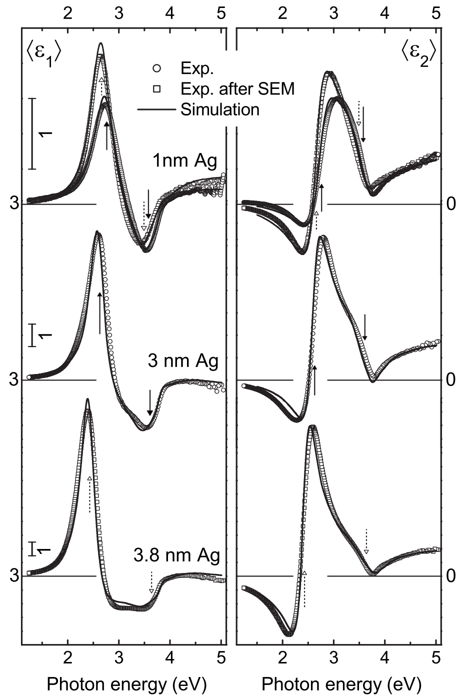

FIG. 6. Real (left) and imaginary (right) parts of the effective dielectric functions $\langle \varepsilon \rangle$ for Ag films on $Al_2O_3(10\bar{1}0)$. Circles and squares correspond to experimental data recorded either before or after SEM measurements, respectively. Solid lines represent simulated spectra.

results reported by Johnson and Christy.[45] We employed the usual correction to the electron relaxation time due to limited size of the particles $1/\tau = 1/\tau_B + (1+a)v_F/R_\parallel$, where τ_B is the bulk relaxation time,[45] v_F is the Fermi velocity, and a is an interfacial damping parameter. We have used $a=0.6$ as reported for Ag on alumina.[46] For the surrounding dielectric shell [Eq. (3)] we used a value $\varepsilon_p=3$ and a thickness d_p depending on the degree of tarnishing or contamination. In this way the spectrum of the nominally 1 nm Ag layer can be reproduced in excellent agreement with the experiment for both stages of tarnishing. The parameters employed in the model are shown in Table I. The rigid redshift of both plasmon modes (compare the position of the dashed arrows with respect to the solid ones) is a direct consequence of the shell thickening, but the line shape at the lower energy side can only be explained by a distortion of the particles, i.e., more truncated spheroids were required to simulate the spectra recorded after the SEM measurements. The actual energy positions of the resonances were reproduced by increasing the effective interaction length $\zeta\langle d \rangle$ to reduce the splitting; here $\langle d \rangle = 1/\sqrt{\rho}$ is the mean center to center cluster spacing and ζ is a free parameter. $\zeta\langle d \rangle$ is used in the Heaviside step function that represents the two-particle distribution function. The fact that this effective interaction distance is smaller than $\langle d \rangle$ has been addressed in the past.[47] The simulated spectra are in good agreement with the experimental data and allow us to identify the spectral position of the (1,0) and (1,1) particle-plasmon modes indicated in Fig. 6 by the arrows (see also Fig. 2). From the simulation of the experimental spectra we also find that the clusters evolve from near spherical to more oblate figures with increasing nominal film thickness, as demonstrated by the monotonously increasing shape ratio[10] $S_t = 2S_z/(1+t)$ in Table I. This is in agreement with previous reports.[48] Variations in the parameters R_z, t, and ζ by $\pm 5\%$ lead to slight but observable distortions in the line shapes and (asymmetric) energy shifts of the order of ± 100 meV (± 20 meV for ζ) for the (1,1) mode and ∓ 5 meV (∓ 20 meV for R_z) for the (1,0) mode.

In Fig. 7 we present RD spectra recorded in UHV conditions for the nominally 1 and 3 nm thick Ag layers. It is noted that the characteristic features consist of negative peaks departing from the background birefringence of the

TABLE I. Parameters used for the simulation of the SE and RD spectra. $R_\parallel$ is the average in-plane radius of the particles, R_z the perpendicular radius, t the truncation parameter, d_p the shell thickness, ρ the cluster number density, S_t the shape ratio, ζ an adjustable parameter for the mean interaction distance, and S_{XY} the in-plane aspect ratio.

Parameter	1 nm Ag			3 nm Ag		3.8 nm Ag
	RDS[a]	SE[b]	RDS/SE[c]	RDS[a]	SE[b]	SE/RDS[c]
$\langle R_\parallel \rangle$ (nm)[d]	3.0	2.93	2.93	6.48	6.44	7.55
$\langle R_\perp \rangle$ (nm)[e]	2.75	2.69	2.69	5.7	5.5	5.7
t [e]	0.54	0.54	0.495	0.6	0.6	0.62
d_p (nm)[e]		−0.07	0.3		−0.04	0.6
$\rho(\mathrm{nm}^{-2})$ [d]	0.007	0.007	0.007	0.002	0.002	0.0016
S_t [f]	1.406	1.415	1.457	1.421	1.464	1.63
ζ [e]	0.4	0.4	0.48	0.41	0.39	0.45
S_{XY} [d]				0.86		0.87

[a] *In situ.*
[b] *Ex situ.*
[c] *Ex situ*, after SEM.
[d] After Fig. 5 ($R_\parallel = R_F$).
[e] Fitted.
[f] Derived.

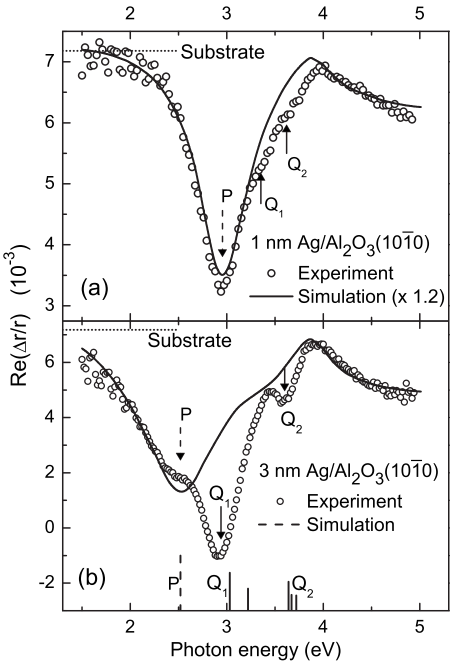

FIG. 7. Experimental RD spectra for (a) 1 nm and (b) 3 nm Ag deposited on the $Al_2O_3(10\bar{1}0)$ surface (circles). The substrate birefringence is indicated by the dotted line. Solid lines are simulations based on the dipole approximation. For comparison the position and relative intensities of the multipolar resonances calculated by Lazzari *et al.* (Ref. 51) are shown as vertical lines at the bottom of (b). The dashed lines indicate dipolar (P) and the solid lines quadrupolar (Q) contributions. The arrows show the main features in the present experiment.

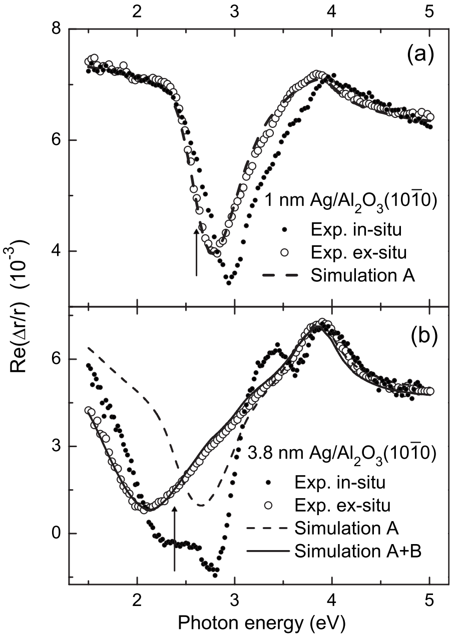

FIG. 8. Comparison of RD spectra recorded *ex situ* (hollow circles) and *in situ* (dots) for (a) 1 nm Ag and (b) 3.8 nm Ag. Simulation A (dashed lines) includes screening and anisotropic image effects. The arrows show the peak position of Eq. (11) (screening contribution) alone. For the simulation $A+B$ in (b) the effect of anisotropic cluster shapes has been included (see text).

substrate indicated by the dotted lines in Fig. 7. In the following we will provide an interpretation of these line shapes invoking the coupling of the polarizability of the cluster to its own anisotropic image and neglecting provisionally in the model any *structural* sources of in-plane anisotropy. Indeed, Figs. 5(a) and 5(d) show that the clusters for the 1 nm Ag layer are statistically isotropic, i.e., the base of the particles is nearly circular with no preferred direction of elongation and they are distributed on the substrate in a stochastic way. This is in contrast to situations in which the clusters clearly show preferential orientation of shapes or high regularity in their distribution.[8,25,44] Yet, a number of previous studies[4,5,12,49,50] have concluded that the dielectric function of the substrate plays an important role in tuning the resonances of the system when the particles are in contact with the substrate. In Fig. 7(a) we present the result of a simulation of the real part of the RD spectrum of 1 nm Ag. By means of Eq. (10), we can reproduce the line shape, sign, and offset of the experimental RD signal—as shown in Fig. 7(a)—by assuming a rigorously isotropic planar geometry. It is worthwhile noting that the resulting amplitude is also comparable to the experiment (1:1.2 ratio). According to Fig. 3, the RD spectrum is apparently dominated by the screening contribution of Eq. (11); however, neglecting the intrinsic contribution of Eq. (12) does not give a good agreement with the experiment. In the absence of a pronounced structural anisotropy we conclude that the anisotropic image effect [Eq. $(12)|_{IM}$] is the key to explain this residual contribution. In the calculation, the imaginary part of the $(1,1)_x$ and $(1,1)_y$ polarizabilities are separated by 2.5 meV, only, and the amplitudes differ by less than 1%. This, however, is enough to be clearly detected by RDS. The most important deviations are the absence in the calculation of the kinks at 3.3 and 3.64 eV in the experimental spectrum, labeled Q_1 and Q_2 in Fig. 7(a), which can be explained by the presence of multipolar resonances.[51] These become more evident at higher coverages as seen in Fig. 7(b), where the RD spectrum for 3 nm Ag is plotted together with a simulation based on the dipole approximation. The simulation even accounts for the average anisotropic shape of the clusters with an in-plane aspect ratio $S_{XY}=R_Y/R_X$ of 0.86. To this end, Eq. $(12)|_{SH}$ was included in the simulation as discussed in the final part of the paper. Still, the calculation clearly fails to reproduce the Q features in the experimental RD spectrum. For comparison, the positions and relative intensities of the multipolar resonances as calculated by Lazzari *et al.*[51] for a Ag nanohemisphere on $\alpha-Al_2O_3$ are indicated at the bottom of Fig. 7(b). These resonances (Q_1, Q_2) originate from the accumulation of polar charges in the sharp triple interface cluster-substrate-medium (vacuum). While the effect of the quadrupolar resonances can be clearly identified experimentally, its modeling is beyond the limits of the present dipolar approach.

However, as evidenced in Fig. 8, there is an efficient way to suppress the quadrupolar resonances by simply exposing the samples of Fig. 7 to air. Upon removal from UHV the particles are partially tarnished and the sharp interfaces responsible for multipolar resonances are smoothened.[51] This, by the way, is the reason why multipolar contributions are also not observed in the SE spectra (Fig. 6) which were all recorded *ex situ*. As discussed above, the primary effect of tarnishing is not only the formation of a dielectric shell around the cluster leading to a rigid redshift of the plasmon modes but also a distortion of the shape of the particles. The corresponding parameters are listed in Table I and are the same for the SE and RDS simulations shown in the top panel of Fig. 6 and in Fig. 8(a), respectively. The simulation of the RD spectrum for the 1 nm Ag layer in Fig. 8(a) now reproduces quite well the experimental curve recorded *ex situ* and after SEM imaging, even the contribution of the Ag bulk interband transition at around 3.9 eV. Although this contribution already influences the position of the resonances for particles much smaller than those presented here,[52] it is not clearly visible in Fig. 7(a) due to the presence of the pronounced multipolar resonances for the *in situ* measurement. For clusters made of noble metals the quadrupolar interaction with the substrate is expected to be rather small;[31] nonetheless, it should survive the tarnishing effect just as the particle-substrate dipolar interaction. This might help us to explain the remaining deviation of the simulation from the experiment at 3.3 eV seen in Fig. 8(a). Again, the experimental RDS line shape and the peak position cannot be reproduced by the screening effect alone, as shown by the arrow in Fig. 8(a), indicating the position of the peak as derived exclusively from Eq. (11): the apparently sharper onset of the resonance at the low energy side (~2.4 eV) can only be modeled by introducing more truncated figures (smaller t) as reported in Table I, which also implies a stronger contribution of Eq. $(12)|_{\mathrm{IM}}$ to the overall spectrum due to the closer distance of the dipoles to their anisotropic images.

Upon exposure to ambient air also the shape related Q features for the thicker films have vanished, as seen in Fig. 8(b) for the 3.8 nm layer sample, thus revealing the contribution of the dipolar resonance. Yet, simulation A, which comprises only the screening and intrinsic image effects $[\mathrm{Eq.}\ (11)+\mathrm{Eq.}\ (12)|_{\mathrm{IM}}]$ and again uses the same parameters as the corresponding SE simulation (lower panel of Fig. 6) yields a very poor match for energies below 3.3 eV. However, this deviation can be mostly corrected by simulation $A+B$ in Fig. 8(b), which includes the in-plane anisotropic cluster shapes $[\mathrm{Eq.}\ (12)|_{\mathrm{SH}}]$, as suggested by the FFT-SEM image of Fig. 5(c). For easier comparison, we have plotted in Fig. 9 the residual spectrum (circles) after subtracting simulation A from the experimental curve of Fig. 8(b). The solid line was produced by considering an *in-plane* aspect ratio $S_{XY}=0.87$, which is the one derived from the FFT-SEM image of Fig. 5(c), while keeping the volume of the particle constant. Here we are not attempting to reproduce the actual amplitude of the spectrum but only the line shape. The amplitude and sign of the signal can be affected by the angle of the axis of preferential orientation with respect to the RD instrument alignment (~−55°) and by the fact that only a small fraction of particles show this orientation. Note that the splitting of the maximum- and minimum-energy positions depends on the aspect ratio (dashed lines) and that the measured S_{XY} nicely reproduces the line shape of the residual spectrum.

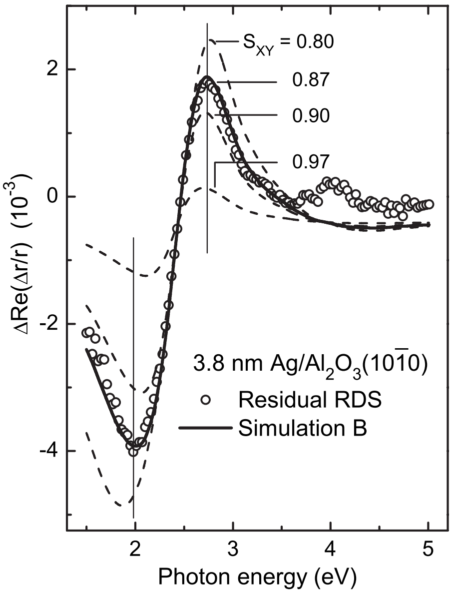

FIG. 9. Residual RDS intensity (circles) obtained as the difference between the measured RD spectrum (*ex situ*) and simulation A in Fig. 8(b) for 3.8 nm $\mathrm{Ag/Al_2O_3(10\bar{1}0)}$. The solid line represents the contribution of the anisotropic cluster shape for an in-plane aspect ratio $S_{XY}=0.87$ as derived from Fig. 5(c). Calculations for several other values of S_{XY} are shown by dashed lines.

It might be surprising that the anisotropy of the quadrupolar resonances is apparently larger than the dipolar one; however, the behavior of the resonances upon tarnishing and the fact that the spectrum of Fig. 8(b) was well simulated using matching SE curves and independently measured aspect ratios lead us to believe that our peaks assignment is correct.

V. CONCLUSION

In summary, SE and RDS have been used to study particle-plasmon resonances of $\mathrm{Ag/Al_2O_3(10\bar{1}0)}$ for nominal Ag layer thicknesses below 4 nm. The RD signal has been explained in terms of two contributions arising due to the birefringence of the substrate: a screening contribution which becomes dominant for overlayers with strong plasmon-related features and an intrinsic anisotropic renormalization of the in-plane polarizabilities due to the dipole images. Both contributions are present even if the individual clusters and their arrangement on the substrate are structurally isotropic. For higher coverages in-plane anisotropic cluster shapes or arrangements and multipolar resonances also contribute to the RD signal. The multipolar resonances can be efficiently quenched by exposing the cluster samples to air.

The combination of RDS and SE allows us to experimentally separate between lateral and out-of-plane anisotropies of particle plasmons. This, together with the quantitative theoretical description presented here, constitutes a sound basis for the optical characterization and control of cluster growth.

ACKNOWLEDGMENTS

We thank J. Winkler and R. Leihmlehner for their expert technical support. We are also indebted to F. Schäffler for access to the SEM facilities. This work was supported by the Austrian Science Fund (FWF) through Contract No. S9002-N20 and the Austrian Nano Initiative (project NSI-MetClust).

---

*peter.zeppenfeld@jku.at

[1] U. Kreibig and M. Vollmer, *Optical Properties of Metal Clusters*, Springer Series in Materials Science Vol. 25 (Springer-Verlag, Berlin, 1995).
[2] C. F. Bohren and D. R. Huffman, *Absorption and Scattering of Light by Small Particles* (Wiley, New York, 1983).
[3] D. Bedeaux and J. Vlieger, *Optical Properties of Surfaces* (Imperial College Press, London, 2002).
[4] T. Yamaguchi, S. Yoshida, and A. Kinbara, Thin Solid Films **21**, 173 (1974).
[5] R. G. Barrera, M. del Castillo-Mussot, G. Monsivais, P. Villaseñor, and W. L. Mochán, Phys. Rev. B **43**, 13819 (1991).
[6] S. Linden, J. Kuhl, and H. Giessen, Phys. Rev. Lett. **86**, 4688 (2001).
[7] N. Esser, A. M. Frisch, A. Röseler, S. Schintke, C. Goletti, and B. O. Fimland, Phys. Rev. B **67**, 125306 (2003).
[8] N. Witkowski, Y. Borensztein, G. Baudot, V. Repain, Y. Girard, and S. Rousset, Phys. Rev. B **70**, 085408 (2004).
[9] S. Chandola, J. Jacob, K. Fleischer, P. Vogt, W. Richter, and J. F. McGilp, J. Phys.: Condens. Matter **18**, 6979 (2006).
[10] R. Lazzari, I. Simonsen, D. Bedeaux, J. Vlieger, and J. Jupille, Eur. Phys. J. B **24**, 267 (2001).
[11] M. Wind, J. Vlieger, and D. Bedeaux, Physica A **141**, 33 (1987).
[12] I. Simonsen, R. Lazzari, J. Jupille, and S. Roux, Phys. Rev. B **61**, 7722 (2000).
[13] B. N. J. Persson and A. Liebsch, Phys. Rev. B **28**, 4247 (1983).
[14] H. Wormeester, A. I. Henry, E. S. Kooij, B. Poelsema, and M. P. Pileni, J. Chem. Phys. **124**, 204713 (2006).
[15] N. Pinna, M. Maillard, A. Courty, V. Russier, and M. P. Pileni, Phys. Rev. B **66**, 045415 (2002).
[16] R. Lazzari, J. Jupille, and Y. Borensztein, Appl. Surf. Sci. **142**, 451 (1999).
[17] D. E. Aspnes, J. P. Harbison, A. A. Studna, and L. T. Florez, J. Vac. Sci. Technol. A **6**, 1327 (1988).
[18] O. Acher and B. Drévillon, Rev. Sci. Instrum. **63**, 5332 (1992).
[19] L. F. Lastras-Martínez, A. Lastras-Martínez, and R. E. Balderas-Navarro, Rev. Sci. Instrum. **64**, 2147 (1993).
[20] P. Weightman, D. S. Martin, R. J. Cole, and T. Farrell, Rep. Prog. Phys. **68**, 1251 (2005).
[21] D. E. Aspnes, Phys. Rev. B **41**, 10334 (1990).
[22] L. F. Lastras-Martínez, J. M. Flores-Camacho, R. E. Balderas-Navarro, M. Chavira-Rodríguez, A. Lastras-Martínez, and M. Cardona, Phys. Rev. B **75**, 235315 (2007).
[23] C. Goletti, G. Bussetti, R. E. Chiaradia, A. Sassella, and A. Borghesi, Appl. Phys. Lett. **83**, 4146 (2003).
[24] S. D. Stookey and R. J. Araujo, Appl. Opt. **7**, 777 (1968).
[25] E. Fort, C. Ricolleau, and J. Sau-Pueyo, Nano Lett. **3**, 65 (2003).
[26] W. Rechberger, A. Hohenau, A. Leitner, J. R. Krenn, B. Lamprecht, and F. R. Aussenegg, Opt. Commun. **220**, 137 (2003).
[27] J. Müller, C. Sönnichsen, H. von Poshinger, G. von Plessen, T. A. Klar, and J. Feldmann, Appl. Phys. Lett. **81**, 171 (2002).
[28] S. Y. Park and D. Stroud, Appl. Phys. Lett. **85**, 2920 (2004).
[29] R. G. Barrera, J. Giraldo, and W. L. Mochán, Phys. Rev. B **47**, 8528 (1993).
[30] H. Hövel, S. Fritz, A. Hilger, U. Kreibig, and M. Vollmer, Phys. Rev. B **48**, 18178 (1993).
[31] C. Beitia, Y. Borensztein, R. Lazzari, J. Nieto, and R. G. Barrera, Phys. Rev. B **60**, 6018 (1999).
[32] R. M. A. Azzam and N. M. Bashara, *Ellipsometry and Polarized Light* (North-Holland, Amsterdam, 1987).
[33] R. Lazzari and I. Simonsen, Thin Solid Films **419**, 124 (2002).
[34] D. Bedeaux and J. Vlieger, Physica (Amsterdam) **67**, 55 (1973).
[35] L. Mochán and R. G. Barrera, Phys. Rev. B **23**, 5707 (1981).
[36] A. Bagchi, R. G. Barrera, and A. K. Rajagopal, Phys. Rev. B **20**, 4824 (1979).
[37] T. Yamaguchi, S. Yoshida, and A. Kinbara, Thin Solid Films **18**, 63 (1973).
[38] S. C. Schneider, S. Grafström, and L. M. Eng, Phys. Rev. B **71**, 115418 (2005).
[39] I. V. Lindell, K. I. Nikoskinen, and A. Viljanen, IEE Proc.: Sci., Meas. Technol. **144**, 156 (1997).
[40] I. V. Lindell, K. I. Nikoskinen, and M. J. Flykt, Radio Sci. **31**, 1361 (1996).
[41] U. Rossow, L. Mantese, and D. E. Aspnes, Appl. Surf. Sci. **123-124**, 237 (1998).
[42] D. Wilcox, B. Dove, D. McDavid, and D. Greer, University of Texas Health Science Center at San Antonio, *Image Tool* (1995), URL: ftp://maxrad6.uthscsa.edu.
[43] I. Horcas, R. Fernández, J. M. Gómez-Rodríguez, J. Colchero, J. Gómez-Herrero, and A. M. Baro, Rev. Sci. Instrum. **78**, 013705 (2007).
[44] S. Camelio, D. Babonneau, D. Lantiat, and L. Simonot, Europhys. Lett. **79**, 47002 (2007).
[45] P. B. Johnson and R. W. Christy, Phys. Rev. B **6**, 4370 (1972).
[46] A. Hilger, M. Tenfelde, and U. Kreibig, Appl. Phys. B: Lasers Opt. **73**, 361 (2001).
[47] S. Norrman, T. Andersson, C. G. Granqvist, and O. Hunderi, Phys. Rev. B **18**, 674 (1978).
[48] T. Wenzel, J. Bosbach, F. Stietz, and F. Träger, Surf. Sci. **432**, 257 (1999).
[49] P. Royer, J. P. Goudonnet, R. J. Warmack, and T. L. Ferrell, Phys. Rev. B **35**, 3753 (1987).
[50] A. Pinchuk, A. Hilger, G. von Plessen, and U. Kreibig, Nanotechnology **15**, 1890 (2004).
[51] R. Lazzari, S. Roux, I. Simonsen, J. Jupille, D. Bedeaux, and J. Vlieger, Phys. Rev. B **65**, 235424 (2002).
[52] A. Liebsch, Phys. Rev. B **48**, 11317 (1993).